

Detection of Undeclared EV Charging Events in a Green Energy Certification Scheme

Luca Domenico Loiacono^{1,2}, Anthony Quinn^{1,3}, Emanuele Crisostomi², Robert Shorten¹

¹Dyson School of Design Engineering, Imperial College London

²Department of Energy, Systems, Territory and Constructions Engineering, University of Pisa

³Department of Electronic and Electrical Engineering, Trinity College Dublin

Abstract

The green potential of electric vehicles (EVs) can be fully realized only if their batteries are charged using energy generated from renewable (i.e. green) sources. For logistic or economic reasons, however, EV drivers may be tempted to avoid charging stations certified as providing green energy, instead opting for conventional ones, where only a fraction of the available energy is green. This behaviour may slow down the achievement of decarbonisation targets of the road transport sector. In this paper, we use GPS data to infer whether an undeclared charging event has occurred. Specifically, we construct a Bayesian hypothesis test for the charging behaviour of the EV. Extensive simulations are carried out for an area of London, using the mobility simulator, SUMO, and exploring various operating conditions. Excellent detection rates for undeclared charging events are reported. We explain how the algorithm can serve as the basis for an incentivization scheme, encouraging compliance by drivers with green charging policies.

Keywords: Electric vehicle (EV), Off-shoring, Green energy certification, Incentivization scheme, Undeclared EV charging, State-of-charge (SoC), Global positioning system (GPS), SUMO, Bayesian hypothesis testing.

1 Introduction

Electric vehicles (EVs) are emerging as pivotal solutions to mitigate urban air pollution, particularly when they replace conventional internal combustion engine (ICE) vehicles. According to the IEA's 2023 Global Electric Vehicle Outlook [13], the global adoption of EVs is accelerating, and, by 2030, under current policies, EVs are expected to comprise about one-third of cars in China and approximately one-fifth in both the United States and the European Union.

The benefits of EVs—in terms of reduced tail-pipe emissions—are undeniable, particularly for people living in urban centres. However, the full potential of EVs can be realised only if renewable energy sources are used in EV charging. Only then will the uptake of EVs actually contribute to the significant decarbonisation of the future road transport sector, while providing co-benefits in terms of reduced air pollution¹.

A failure to guarantee the utilization of renewable energy in EV charging leads to the *off-shoring* of emissions [38]. Off-shoring refers to the shifting of pollution from an EV's location in a *source* country

¹<https://www.eea.europa.eu/publications/electric-vehicles-and-the-energy>

This work has been submitted to the IEEE for possible publication. Copyright may be transferred without notice, after which this version may no longer be accessible.

or region to a different—often geographically far removed— *host* country or region where the electric energy used to charge its battery is actually generated. The negative impact of this practice becomes particularly significant if the electric energy is derived from fossil fuels (e.g. coal). Typically, such (polluting) energy production is off-shored to hosts with laxer environmental regulations. Therefore, evaluating the environmental and social justice impacts of EVs is a complex issue that involves understanding how environmental policies and industrial practices affect pollution distribution. Unilateral environmental policies in source countries can reduce *local* emissions by moving emission-intensive production abroad. However, this can lead to an increase in *global* emissions if the host countries have less stringent regulations, such as a heavy reliance on fossil fuels for electricity generation [15].

Central to these concerns is whether EVs actually provide any carbon footprint advantage over ICE vehicles, when the EV's production and end-of-life phases are accounted for. Analysis² of Polestar 2 EV variants, for instance, has shown that—in order to break even against the Volvo XC40 ICE vehicle—their required use phase (i.e. distance travelled) varies enormously depending of the combination of EV variant and the electricity mix they use. This ranges from 40,000 km for the Polestar 2 standard range single motor EV using wind-generated energy, to 110,000 km for the long range dual motor variant using a global electricity mix.

To address these concerns about EV energy production—offshoring, off-setting, and the electricity mix—and to counter *green hypocrisy* among EV stakeholders, who appear to be environmentally friendly without actually being so, it is crucial to ensure that the energy used for EV charging truly has a green origin, i.e. that it comes from renewable energy sources (RES) [43]. Various methodologies are used to guarantee that charging stations only use energy directly generated from RES to charge EVs, or, more often, that the energy used to charge EVs is offset from generation from RES [3, 8, 25, 35]. We refer to these methodologies collectively as the *certification of green energy*. In this paper, we envisage that *certified charging stations* adhere to a particular green-energy certification scheme, and can, accordingly, incentivize EV drivers/owners (forthwith referred to simply as the driver) who decide to charge at these stations.

For the EV driver, charging at certified charging stations may be expensive or inconvenient when compared to uncertified charging with a generic energy mix, such as in the case of home charging [31]. Accordingly, they may be induced to *hide* such a charging event, in order to avoid a notional penalty associated with uncertified charging, or, alternatively, in order to claim a bonus from a notional incentivization scheme designed to encourage certified charging events. This paper is concerned with detecting whether such *undeclared* (i.e. hidden) charging events have actually occurred between consecutive declared and certified charging events³.

Our design of a detection algorithm for undeclared charging events is based on a key assumption to ensure reliability; i.e. that all data available from the EV, including direct measurements of the state-of-charge (SoC), cannot be used to evaluate whether undeclared charging events have taken place, for the obvious reason that an EV driver who wishes to hide a charging event may be induced also to interfere with the EV's data. Instead, we assume that a GPS device is installed in the EV (as is usually the case for insurance reasons), and we assume that the GPS data are reliable. During a certified charging event, the GPS device communicates to our algorithm the sequence of trips—specifically the time-stamped sequences of speeds and altitudes of the EV during those trips—since the last certified charging event.

The detection algorithm which we develop in this paper is Bayesian, in the sense that it elicits prior probability models for unobserved states, conditions on observations and known states, and constructs

²www.polestar.com/data-assets/11286/1630409045polestar1carapportprintkorr11210831.pdf

³While the most probable reason for a driver to hide a charging event is because it occurred at an uncertified charging point, our algorithm detects only whether an undeclared charging event occurred, and not whether the charge was certified. The idea here is that a *necessary* condition of compliance with an incentivization scheme for certified charging is that every charging event be declared.

a predictive probability model. The latter yields the (detection) probability of an undeclared charging event (or events⁴) having occurred since the last certified charging event (which we will call the *certified interval* between charging). As already stated, we process the GPS data (notably the speed data), and other known parameters of the EV (e.g. mass, battery size, type of heating/cooling device) to predict the actual—but uncertain—energy consumption during the certified interval. Significant (i.e. improbable) deviations of the declared energy consumption from the predictions of the predictive probability model can be flagged, yielding a probability that an undeclared charging event occurred during the certified interval. We report extensive simulations using the mobility simulator, SUMO [4]. We show that the proposed methodology performs well in different seasons of the year (when the uncertainty of using auxiliary heating/cooling devices plays an important role in energy consumption), achieving true negative (i.e. detecting that a compliant driver did not hide a charging event) rates between 98.4% and 99.9%. The true positive rates (i.e. detecting that non-compliant drivers did hide a charging event) reach 100% in the case where the undeclared charge is 50% of the size of the battery. The details are provided in Section 4.

As regulatory focus on off-shoring and energy sourcing intensifies, future policies are expected to consider not just the type of energy consumed by a vehicle, but also the source of that energy [23]. Algorithms such as the one developed in this paper may serve as the enabling mathematical basis to ensure compliance with continuous green charging practices, and with evolving regulatory expectations.

1.1 State of the art

The main objective of this paper is to develop a Bayesian methodology which tests whether drivers are confining their charging events to certified green charging stations, and this can form the basis for a down-stream incentivization scheme. The idea is to test whether the data recorded by the GPS device during a certified interval are consistent with the change (i.e. differential) in the state-of-charge (SoC)—which is an energy quantity—recorded by the consecutive certified charging stations. To the best of our knowledge, this is the first time that this problem has been formulated and discussed. Nevertheless, it is related to the problem of estimating the energy consumed by an EV over a specific route, for which many physics-based and data-driven methodologies have already been proposed in the literature, which we will now review.

It is known that many factors influence EV energy consumption and can cause significant variability over a specified GPS-tracked route, leading to uncertainty in predicting the actual energy consumption. These factors include travel-related aspects, such as distance travelled, speed, acceleration, cumulative change in altitude, and cruising time [6]; environmental factors such as ambient temperature [14, 28]; visibility and wind effects [9]; vehicle-related parameters including mass, and auxiliary energy loads due to heating, ventilation, and air-conditioning (HVAC) [17, 20, 39]; roadway topography such as slope [21]; traffic conditions [22]; and driver-related aspects such as driving behaviours, car-following behaviour, and charging habits [19, 33]. In addition, battery health and degradation effects due to ageing of the EV [42, 44]—and even efficiency of regenerative braking [7, 29]—are typical factors affecting EV energy efficiency. These considerations underscore the importance of comprehensively accounting for diverse variables to develop accurate models of EV energy consumption. While all the aforementioned factors do, indeed, influence the actual EV energy consumption, the most significant are

- (i) the net mass of the loaded EV, which is uncertain as it depends on the undeclared number and masses of the people; and
- (ii) the use of auxiliary power devices in the EV, most notably for heating and cooling purposes.

⁴We do not infer the number of such events, only that one or more has/have occurred.

In our work, these two unobserved states provide the principal sources of uncertainty about the actual energy consumed by a driver during the trips which they undertook in a certified interval. This is consistent with the energy consumption model (reviewed in Section 2) developed in SUMO [4]. SUMO is the popular road traffic simulator that we use in this paper (Section 4) to model our road network and charging station infrastructure, as a means for validation of our methodology [18].

In addition to the literature on estimation of energy consumption, there are related papers on the need to incentivize EV charging via renewable energy sources. A pioneering work in this direction was [12], where the operation of EVs was orchestrated in order to maximise the consumption of energy generated from renewable sources. Recent advances in incentivizing EV charging with RES have led to innovative control algorithms designed to encourage accurate reporting of charging preferences (in terms of time and location) and optimize grid stability. For instance, [16] introduced algorithms that incentivise truthful preference reporting among EV drivers, facilitating better alignment of charging patterns with renewable energy availability. Additionally, [30] developed dynamic control algorithms that adjust incentives based on real-time data, in order to motivate EV drivers to adapt their charging schedules, thereby contributing to the management of grid stability and to congestion avoidance. Similarly, [27] proposed financial rewards to encourage EV users to charge at specific times and locations, aiming to maximize the use of renewable energy and minimize shortages. These previous studies have principally aimed to align EV charging with renewable energy production via financial incentives and real-time adjustments. In contrast, our approach is significantly different as it verifies adherence to incentive schemes by constructing a probability-based predictor of EV energy consumption during a certified interval (i.e. between certified green charging events). This enables the detection of undeclared—and presumably uncertified—charging events, thereby encouraging constant compliance with certified green energy charging practices.

1.2 Layout of the paper and notational conventions

In Section 2, we present our methodology for data-driven stochastic prediction of the actual EV energy consumption during a certified interval. This is used in Section 3 to compute a hypothesis test (detector), which processes the recorded differential SoC during the certified interval into a probability that the driver has hidden (i.e. failed to declare) at least one charging event. Section 4 gives the details of the mobility simulator used for our validating case study, and summarizes the outcomes of the simulations. Finally, Section 5 concludes our manuscript by summarising our findings, noting the downstream role of the methodology in an incentivization scheme for green energy charging, and outlining our current lines of research to extend the presented work.

2 Energy consumption from an EV battery, x_C

In what follows, we review a physical model (Section 2.1) which relates the energy consumed from an EV battery (i.e. drawn from the battery) during a trip (or trips) to the GPS-measurable properties of the trip(s) (Section 2.2), and to a set of known parameters (constants) associated with the specific EV. The model also depends on other unknown (i.e. unobserved) states of the EV, which may vary during and between the trips. These are modelled stochastically in Section 2.3. This will enable construction of a Bayesian predictive model of x_C (Section 3), where x_C is the total energy consumed from the battery during a certified interval.

2.1 Physical model

We adopt the physical model proposed in [18] and implemented in SUMO, in which the total energy consumed by an EV during a trip is computed in a discrete-time manner. In what follows—and in the

simulations in Section 4—we assume a stepsize of 1 s, i.e. $t \in \{0, 1, 2, \dots\}$, and all time-varying quantities (e.g. the speed, $v[t]$) are assumed to be constant during these 1 s time intervals. Where symbols are not defined in place below, they are *known* EV parameters—denoted by θ —which are listed in Table 1.

1. At (absolute) time $t \in \{0, 1, \dots\}$, the (instantaneous) energy of the EV is computed by summing its kinetic, potential, and rotational energy components,

$$\begin{aligned} E_{veh}[t] &= E_{kin}[t] + E_{pot}[t] + E_{rot,int}[t] \\ &= \frac{1}{2}m_{total}[t] \times v^2[t] + m_{total}[t] \times g \times h[t] + \frac{1}{2}J_{int} \times v^2[t], \end{aligned}$$

where $m_{total}[t]$, $h[t]$ and $v[t]$ denote the total mass of the EV, its altitude and speed at time t , respectively, and g is the acceleration due to gravity. We emphasize the discrete nature of the independent time variable, t , by adopting square brackets, $[\cdot]$.

2. The energy required during the (next) time interval, $(t, t + 1]$, is therefore

$$\Delta E_{req}[t] = E_{veh}[t + 1] - E_{veh}[t]. \quad (1)$$

3. The energy consumed in time interval, $(t, t + 1]$, can be calculated as follows:

$$\Delta E_{cons}[t] = \Delta E_{req}[t] + \Delta E_{loss}[t]. \quad (2)$$

Here, the energy loss, ΔE_{loss} , itself consists of three components,

$$\Delta E_{loss}[t] = \Delta E_{air}[t] + \Delta E_{roll}[t] + \Delta E_{aux}[t], \quad \text{where} \quad (3)$$

$$\Delta E_{air}[t] = \frac{1}{2} \times \rho_{air} \times A_{veh} \times c_w \times v^2[t] \times \Delta s[t],$$

$$\Delta E_{roll}[t] = c_{roll} \times m_{total}[t] \times g \times \Delta s[t], \quad (4)$$

$$\Delta E_{aux}[t] = W[t], \quad \text{and} \quad (5)$$

$$\Delta s[t] = v[t]. \quad (6)$$

In (3), $\Delta E_{air}[t]$ and $\Delta E_{roll}[t]$ denote the energy loss in the EV due to air resistance and roll, respectively. They depend on $\Delta s[t]$, i.e. the (absolute path) distance travelled in the 1 s interval, $(t, t + 1]$. Also, $\Delta E_{aux}[t]$ denotes the energy loss due to the use of auxiliary devices and services (e.g. cooling/heating), where $W[t]$ is the average power consumed by these devices and services during the 1 s interval. Finally, ρ_{air} denotes the density of air.

4. $\Delta E_{cons}[t]$ may either be a positive or a negative quantity, since it represents the amount of energy the EV consumes due to its movement. It is negative, for instance, when regenerative braking is used. The energy actually drawn from the battery in the 1 s interval, $(t, t + 1]$, is denoted by $\Delta x[t]$. This depends on constant efficiency factors for the battery (Table 1), i.e. $\eta_{prop} \in (0, 1)$ if $\Delta E_{cons}[t] > 0$ (the *propulsion* case), and $\eta_{recup} \in (0, 1)$ if $\Delta E_{cons}[t] < 0$ (the *recuperation* case). Specifically:

$$\begin{aligned} \Delta x[t] &= \Delta E_{cons}[t] \times \eta_{prop}, \quad \text{if } \Delta E_{cons}[t] > 0, \\ \Delta x[t] &= \Delta E_{cons}[t] \times \eta_{recup}, \quad \text{if } \Delta E_{cons}[t] < 0. \end{aligned} \quad (7)$$

Finally, we define $x_C[t]$ as the *cumulative energy drawn from the battery* in a *net* interval of t s. It is computed as the sum of the energies (7) drawn from the battery in each 1 s interval:

$$x_C[t] = x_C[t - 1] + \Delta x[t - 1], \quad t \in \{1, 2, \dots\}, \quad (8)$$

initialized with $x_C[0] = 0$. This unobserved (i.e. uncertain) time-varying quantity (i.e. state process) is our principal quantity of interest, and we will stochastically model and predict it in Section 3.

Parameter	Symbol	Units
Battery Capacity	E_{max}	kWh
Kerb Mass	m_{veh}	kg
Front Surface Area	A_{veh}	m ²
Internal Moment Of Inertia	J_{int}	kg · m ²
Radial Drag Coefficient	c_{rad}	-
Roll Drag Coefficient	c_{roll}	-
Air Drag Coefficient	c_w	-
Propulsion Efficiency	η_{prop}	-
Recuperation Efficiency	η_{recup}	-

Table 1: EV parameters, θ , used in the physical model (1)-(8).

2.2 GPS-measured quantities, $v[t]$ and $h[t]$

We have seen how $x_C[t]$ —the cumulative energy drawn from the battery during a trip of duration t s—depends on the sequentially measured (i.e. observed) speed and altitude of the EV, $v[t]$ and $h[t]$, respectively. We have assumed that a GPS device provides these measurements. An EV *trip* refers to a distinct segment of driving activity, defined from the moment an EV is switched on until it comes to a complete stop and is switched off. Each trip is assigned a unique numeric label (Table 2). Note that $\Delta t = 1$ s, as assumed in (6). Also, the discrete-time index, $t \in \{1, 2, \dots\}$, is reset to 1 in (8) when the trip number increments, and $x_c[0]$ is re-initialized with the cumulative value attained at the end of the previous trip. In the sequel, \mathbf{d}_G will denote the multi-trip GPS data record for the certified interval.

Trip Number	GPS-time	Speed (v)	Altitude (h)
1	07/07/24 10:23:59	3.4 m/s	0 m
1	07/07/24 10:24:00	1.9 m/s	2 m
1	07/07/24 10:24:01	10.4 m/s	4 m
1	07/07/24 10:24:02	.	.
1	07/07/24 10:24:03	.	.
2	08/07/24 19:03:14	1.1 m/s	30 m
2	08/07/24 19:03:15	5.7 m/s	33 m
2	08/07/24 19:03:16	.	.
2	08/07/24 19:03:17	.	.

Table 2: Extracts from a typical multi-trip GPS data record, \mathbf{d}_G , with $\Delta t = 1$ s.

2.3 Unobserved variables

Evaluation of the cumulative energy drawn from the battery, $x_C[t]$ (8), also depends on other unknown and unmeasured quantities, as follows:

- (i) $m_{total}[t]$, being the *total* mass of the loaded EV at each measurement time, t (1), (4);
- (ii) $W[t]$, the average power consumed by auxiliary services (such as onboard infotainment systems and air-conditioning), at each t (5).

In the next two subsections, we develop (static) probability models for these uncertain processes.

2.3.1 Total mass of the loaded EV, $m_{total}[t]$

The total vehicular mass, $m_{total}[t]$, is given by the sum of the kerb mass, m_{veh} —which is an invariant vehicular parameter (Table 1)—plus the net mass of people (driver plus passengers), $m_{peop}[t]$. In principle, one should also consider the mass of luggage, but we neglect this for simplicity, as it is small compared to that of the people. Importantly, we only model the average mass of the people carried by the EV at *any* time during a trip, eliminating the dependence of $m_{peop}[t]$ on t ; i.e. $m_{peop}[t] \equiv m_{peop}$.

We adopt a Gaussian mixture model (GMM) as the probability model for m_{peop} , where each component models the different possible numbers of people typically carried by the EV, denoted by N_p (to include the driver). The implied hierarchical probability model is as follows:

- **Prior modelling of the number of people carried by the EV**

The prior model for the number of people, $p_k \equiv \Pr[N_p = k]$, $k \in \{1, \dots, 5\}$. This probability mass function (pmf) is inferred using statistical data sourced from [24] and Eurostat statistics [10]. From these sources, the expected number of people per trip is found to be approximately 1.6. The pmf is then constructed with this expected value as a constraint, and assigning strictly decreasing probabilities. With five degrees-of-freedom but only two constraints, the pmf is under-determined. It is chosen as follows, to reflect the available data sources (above):

No. people, $N_p = k$	pmf, p_k
1	0.61
2	0.23
3	0.11
4	0.04
5	0.01

- **Conditional Gaussian modelling of the mass of people**

Given $N_p = k$, the mass of people carried by the EV, m_{peop} , follows a Gaussian distribution:

$$F(m_{peop} | N_p = k) \propto \mathcal{N}(m_{peop} | \mu_k, \sigma_k^2) \quad (9)$$

with $m_{peop} \in \mathbb{R}^+$. We choose the conditional mean to be $\mu_k = k \times 74$, and the conditional standard deviation to be $\sigma_k = 12\sqrt{k}$. The $k = 1$ standard interval (one person) is based on data from [41].

- **Marginal modelling of net mass (of people) carried by EV**

The overall distribution of mass (of people) carried by the EV is therefore the mixture of components (9), weighted by the N_p -probabilities above:

$$F(m_{peop}) = \sum_{k=1}^5 p_k F(m_{peop} | N_p = k). \quad (10)$$

This GMM is depicted in Figure 1.

Figure 1: Gaussian mixture model (GMM), $F(m_{peop})$, of the net mass of people typically carried by an EV during a trip.

2.3.2 Average power consumption of auxiliary devices, $W[t]$

The energy consumed by auxiliary devices, E_{aux} (3), can account for a significant proportion of the total energy consumed by the EV during a trip, E_{cons} (2). E_{aux} is strongly dependent on the time of year, since weather conditions strongly influence the utilization of HVAC (Heating, Ventilation, and Air Conditioning) and the lights [2], [20]. For this reason, we *conditionally* model the unknown and unobserved auxiliary power, W (6), via the observed Bernoulli random variable (r.v.), $Y \in \{s, w\}$. These states denote the case where the trip takes place during the warmer (summer⁵, s) or cooler (winter, w) periods of the year, respectively, a condition easily verified by the GPS time-stamps (Table 2).

Conditional Gamma Modelling of the Auxiliary Power, $W[t]$

As in Section 2.3.1, we facilitate the (conditional) stochastic modelling of the auxiliary power process, $W[t]$, by modelling its *average* value, so that $W[t] \equiv W$ in (6). Since $W \in \mathbb{R}^+$, gamma modelling is appropriate [5]:

$$F(W|Y = y) \equiv \mathcal{Gamma}(k_y, \theta_y). \quad (11)$$

Here, the $y \in \{s, w\}$ -indexed parameters of the gamma model are its shape parameter, $k_y > 0$, and its scale parameter, $\theta_y > 0$, so that the conditional expected value (mean) and conditional variance of W are

$$E[W|Y = y] = k_y \theta_y, \quad \text{Var}[W|Y = y] = k_y \theta_y^2. \quad (12)$$

If these moments are available—for example via test data labelled by season—then the seasonally-conditioned gamma parameters, k_y and θ_y , can be estimated via moment-matching:

$$k_y \equiv \frac{E[W|Y = y]^2}{\text{Var}[W|Y = y]}, \quad \theta_y \equiv \frac{\text{Var}[W|Y = y]}{E[W|Y = y]}. \quad (13)$$

Seasonal quantifiers of expected auxiliary power requirements, $E[W|Y = y]$, are available in the literature [11], [32], [37], but we were not able to source the variances, $\text{Var}[W|Y = y]$. Therefore, we adjusted the latter, constrained by the former (for each period of the year) to ensure a good fit of the published empirical data for W (Figure 2), yielding the following conditional gamma parameters via (13):

	Scale θ_y	Shape k_y	$E[W Y = y]$
Winter ($Y = w$)	800	3	2400 W
Summer ($Y = s$)	400	2	800 W

⁵In this paper, *summer* might best be understood as *not winter*, as far as the London context of the SUMO simulation is concerned (Section 4.1). In that city, we associate summer with a low usage of any auxiliary services, and winter with high usage of heating and lights. In other climates, of course, the high- and low-usage periods of the year may be delimited differently.

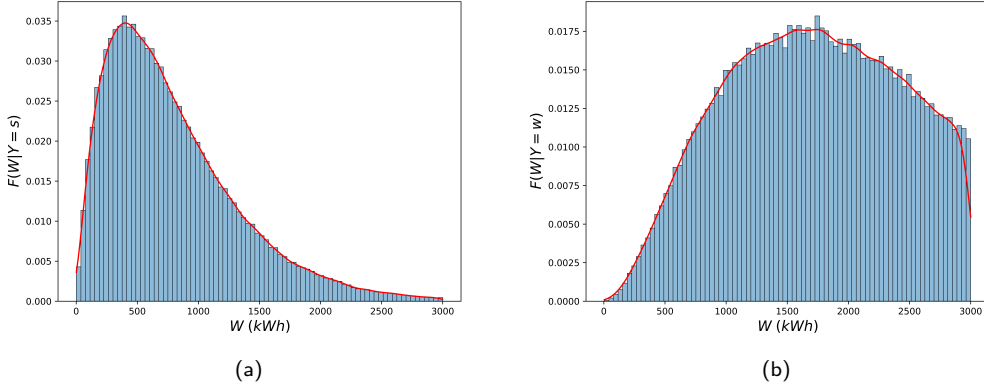


Figure 2: Gamma models, $F(W | Y = y)$, of the average power consumed by the auxiliary devices and services of an EV during a trip in (a) summer ($Y = s$), and (b) winter ($Y = w$).

3 The probability, $\Pr[H_1 | \mathbf{d}_G, \theta, y, x_D]$, of undeclared charging during a certified interval

We now develop the main result of the paper, which is a hypothesis test for compliance with a notional green-energy charging scheme. Specifically, we evaluate the probability of the proposition, $H_1 \equiv$ *the EV was charged during a specific (i.e. the last⁶) certified interval, without such charging event(s) having been declared*. This hypothesis test, yielding

$$0 < \Pr[H_1 | \mathbf{d}_G, \theta, y, x_D] < 1, \quad (14)$$

is to be implemented at the current certified charging station in order to detect whether undeclared charging occurred (for example, at home) at least once since the last certified charging event. Since any undeclared charging event(s) cannot be certified by the green-energy scheme, this hypothesis test (14) can be used to withhold an incentive from—or even apply a penalty to—the driver under that scheme.

When the EV connects at a certified charging station, we assume that the H_1 -testing algorithm can access the multi-trip GPS data, \mathbf{d}_G (Table 2), collected from all the trips that occurred during the certified interval. This, of course, means that the season, $Y = y \in \{s, w\}$ (11), is also known. Furthermore, we assume that the specific EV model is recognized, and so its parameters, θ (Table 1), can be looked up by the algorithm.

Finally, and crucially, the charging station senses the (absolute) SoC (a measure of energy, in kWh) of the EV immediately after it is plugged in. We denote this by x_1 . The algorithm must also have access to the SoC of the EV which was recorded immediately after charging at the previous certified charging station, i.e. x_0 . The certified *differential SoC*, $x_D \equiv x_0 - x_1$, is therefore observed (i.e. it appears in the condition of the *a posteriori* probability (14)). The purpose of the H_1 -testing algorithm is to compare x_D to the uncertain cumulative energy actually drawn from the battery during that interval, $x_C^{[T_c]} \equiv x_C$ (8) (where T_c denotes the cumulative time of all the trips taken during the certified interval⁷). This probabilistic

⁶We envisage that the test is implemented at every charging station belonging to the specific green energy scheme offering the incentives or applying the penalties of that scheme.

⁷We will refer to T_c simply as the *certified interval duration*, with the understanding that the time counter is reset at the beginning of each trip, as explained at the beginning of Section 2.2.

comparison is inferentially equivalent to the soft (i.e. Bayesian) classification of x_D . Therefore, we must first construct the distribution of uncertain x_C by processing (i.e. conditioning on) the entire knowledge base at the start of charging, this being $\mathbf{d}_G, \theta, Y = y$, along with the uncertainty models (i.e. probability distributions), $F(m_{peop})$ (10) and $F(W|Y = y), y \in \{s, w\}$ (11). We now present the various steps involved in constructing this test.

3.1 The battery energy conservation equation

The observed SoC of the EV battery immediately after the *previously* certified charging event, x_0 , and immediately before charging commences during the *current* certified charging event, x_1 , are related to the (unobserved and uncertain) cumulative energy drawn from the battery during that interval, x_c , via the following energy conservation equation⁸:

$$x_0 - x_1 \equiv x_D \equiv x_C - x_U > 0. \quad (15)$$

Here, x_U denotes the total amount of energy provided to the battery by undeclared charging events during the certified interval. We make the following key simplifying stochastic modelling assumption in respect of the r.v.s, x_C and x_U :

$$x_C \perp\!\!\!\perp x_U,$$

i.e. the amount of undeclared charging is independent of the cumulative energy drawn from the battery. We will use this assumption to elicit the distributions of x_C and x_U *independently*, in the next two subsections, respectively.

3.2 Empirical probability model of x_C , the cumulative energy drawn from the battery

The physical model (1)-(8) relates x_C *deterministically* to the *observed* data (i.e. the GPS record, \mathbf{d}_G), the *known* EV-specific parameters, θ (Table 1), the *known* season, $Y = y \in \{s, w\}$, but also to the *unknown* and unobserved quantities, m_{peop} (10) and W (11); i.e.

$$x_C \equiv g(\mathbf{d}_G, \theta, y, m_{peop}, W),$$

with $g(\cdot)$ specified by (1)-(8). Hence, x_C is unknown (i.e. a r.v.), whose distribution we now seek. Having elicited the marginal probability models of m_{peop} and W , we assume—reasonably—that they are stochastically independent, i.e. $m_{peop} \perp\!\!\!\perp W$. Formally, then, our entire knowledge base is processed consistently into *marginal* inference of unknown x_C —having marginalized over the unknowns—as follows:

$$F(x_C | \mathbf{d}_G, \theta, y) = \int_0^\infty \int_0^\infty \delta(x_C - g(\mathbf{d}_G, \theta, y, m_{peop}, W)) F(m_{peop}) F(W | y) dW dm_{peop}. \quad (16)$$

We construct the standard empirical approximation [34] of this distribution via a random sample of size $n \gg 0$, from $F(m_{peop})$ (10) and $F(W | y)$ (11):

$$\tilde{F}(x_C | \mathbf{d}_G, \theta, y) \equiv \frac{1}{n} \sum_i \delta(x_C - g(\mathbf{d}_G, \theta, y, m_{peop}^{(i)}, W^{(i)})), \quad (17)$$

⁸ Detection of undeclared charging is trivial when $x_D \leq 0$, since, then, $x_U \geq x_C > 0$.

where

$$\begin{aligned} m_{peop}^{(i)} &\sim F(m_{peop}), \\ W^{(i)} &\sim F(W | y). \end{aligned}$$

We will use (17) to predict x_C for a particular EV model, θ , with GPS record, \mathbf{d}_G , operating in a particular season, $Y = y \in \{s, w\}$. The seasonality of this predictive distribution of energy drawn from the EV battery is evident in the examples displayed in Figure 3. Note that the support of the empirical approximation (17) is the random sample, $\{x_C^{(1)}, \dots, x_C^{(n)}\}$, where

$$x_C^{(i)} \equiv g(\mathbf{d}_G, \theta, y, m_{peop}^{(i)}, W^{(i)}), \quad i = 1, \dots, n. \quad (18)$$

In Fig. 3, we display the histograms formed by uniformly binning these iid (i.e. independent, identically distributed) samples to (quantized) values, \hat{x}_C . This reveals the form of the underlying pdfs (16).

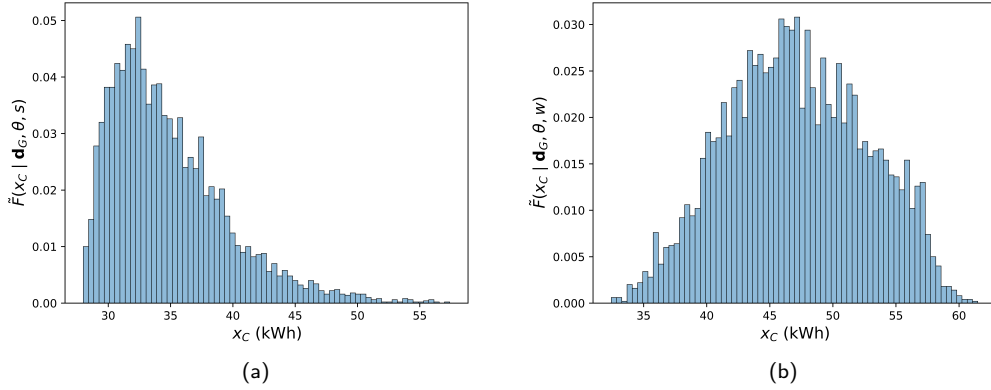


Figure 3: Histograms of empirical distributions of the energy drawn from the battery, $\tilde{F}(x_C | \mathbf{d}_G, \theta, y)$, for (a) summer ($y = s$), and (b) winter ($y = w$).

3.3 Probability model of x_U , the undeclared energy

The net amount of undeclared energy, x_U , supplied to the EV battery during the certified interval is, by definition, unknown. Its distribution has two components, conditional on the behaviour of the driver, as follows:

$$\begin{aligned} H_1 &: \text{at least one undeclared charging event occurred } (\Pr[H_1] \equiv p_1), \\ H_0 \equiv \overline{H_1} &: \text{no undeclared charging event occurred } (\Pr[H_0] \equiv p_0 = 1 - p_1). \end{aligned} \quad (19)$$

Here, p_1 is the *a priori* probability that the driver engaged in undeclared charging. The primary focus of this paper is to update this probability—using Bayesian inference, as explained in the sequel—to its data-driven *a posteriori* value (14), having processed the specific EV data from the last certified interval.

In the H_1 case, we adopt the conservative uniform distribution in the interval, $I_U \equiv (0, \bar{x}_U]$ (kWh), where \bar{x}_U is the maximum possible amount of undeclared energy⁹:

$$F(x_U | H_1) \equiv \mathcal{U}_{I_U}(x_U). \quad (20)$$

⁹ For instance, \bar{x}_U equals the (energy) capacity of the EV battery, E_{max} (Table 1), if we assume that only one undeclared

Conversely, $x_U \stackrel{\text{a.s.}}{=} 0$ in the H_0 case:

$$F(x_U | H_0) \equiv \delta(x_U). \quad (21)$$

Hence, the marginal model of x_U is the slab-and-spike distribution:

$$F(x_U) \equiv p_1 \mathcal{U}_{I_U}(x_U) + (1 - p_1) \delta(x_U). \quad (22)$$

3.4 Induced distribution of certified differential SoC, x_D

The energy conservation equation (15) expresses the observed x_D (i.e. the certified differential SoC) as the difference between the two unobserved energy quantities, i.e. $x_C \sim \tilde{F}(x_C | \cdot)$ (17) (the cumulative energy drawn from the battery) and $x_U \sim F(x_U)$ (22) (the undeclared energy), respectively. Analysis is greatly facilitated by our assumption of independence between these quantities. In this case, the induced *a posteriori* distribution of x_D —i.e. *after* processing the EV-specific evidence, \mathbf{d}_G , θ and $y \in \{s, w\}$, from the certified interval—is the *deterministic correlation* of $\tilde{F}(x_C | \cdot)$ and $F(x_U)$ [1]:

$$\begin{aligned} \tilde{F}(x_D | \mathbf{d}_G, \theta, y) &= \tilde{F}(x_C | \mathbf{d}_G, \theta, y) * F(-x_U)|_{x_C \rightarrow x_D, x_U \rightarrow x_D} \\ &= p_1 \tilde{F}(x_C | \mathbf{d}_G, \theta, y)|_{x_C \rightarrow x_D} * \mathcal{U}_{I_U}(-x_D) + (1 - p_1) \tilde{F}(x_C | \mathbf{d}_G, \theta, y)|_{x_C \rightarrow x_D} \\ &= p_1 \tilde{F}(x_D | \mathbf{d}_G, \theta, y, H_1) + (1 - p_1) \tilde{F}(x_D | \mathbf{d}_G, \theta, y, H_0). \end{aligned} \quad (23)$$

This is a binary mixture model with components,

$$\tilde{F}(x_D | \mathbf{d}_G, \theta, y, H_1) \equiv \tilde{F}(x_C | \mathbf{d}_G, \theta, y)|_{x_C \rightarrow x_D} * \mathcal{U}_{I_U}(-x_D), \quad (24)$$

$$\tilde{F}(x_D | \mathbf{d}_G, \theta, y, H_0) \equiv \tilde{F}(x_C | \mathbf{d}_G, \theta, y)|_{x_C \rightarrow x_D}. \quad (25)$$

These components are conditioned on the hypothesis of interest (19) being true, i.e. H_1 , and false, i.e. H_0 , respectively. The mixing probabilities, p_1 and $1 - p_1$, are the *a priori* probabilities of these hypotheses (see footnote 9), and $*$ denotes linear convolution. For convenience, we compute $\tilde{F}(x_D | \mathbf{d}_G, \theta, y, H_1)$ by discretizing $\mathcal{U}_{I_U}(x_U)$ —denoted by $\tilde{\mathcal{U}}_{I_U}(x_U)$ —to the same bins, \hat{x}_C —as those used for $\tilde{F}(x_C | \cdot)$ (17) (see Fig. 3), yielding the discrete correlation,

$$\tilde{F}(\hat{x}_D | \cdot, H_1) = \tilde{F}(\hat{x}_D | \cdot) * \mathcal{U}_{I_U}(-\hat{x}_D) \equiv \sum_{\hat{x}_U \in I_U} \tilde{F}(\hat{x}_U | \cdot) \times \tilde{\mathcal{U}}_{I_U}(\hat{x}_U + \hat{x}_D). \quad (26)$$

Remark (Range of x_D). *Let the actual range of $x_C > 0$ —i.e. the support of distribution (17)—be $I_C \equiv (\underline{x}_C, \bar{x}_C)$, and recall that $x_U \in I_U \equiv (0, \bar{x}_U)$. It follows from (23) that $x_D \in I_D \equiv (\underline{x}_D, \bar{x}_D) = (\underline{x}_C - \bar{x}_U, +\bar{x}_C)$. This is best understood by noting that the H_1 -component in (23)—i.e. (24), implemented via (26)—implements a sliding sum of $\tilde{F}(\hat{x}_U | \cdot)$. These bounds for x_D capture the extreme cases reasonably: (i) if $x_C = 0$ (15), then $\bar{x}_U = E_{max}$ (see footnote 9), and so $\underline{x}_D = -x_U = -E_{max}$. Conversely, if $x_U = 0$, then $\bar{x}_C = E_{max}$, and so $\bar{x}_D = \bar{x}_C = E_{max}$.*

Figure 4 displays the binned empirical distributions (i.e. histograms) of x_D , corresponding to the cases in Figure 3.

charging event occurred during the certified interval. We do not actively invoke this assumption.

On a more subtle point, the x_U modelling in (19)-(22) is elicited independently of the EV-specific database; i.e. $F(x_U | \mathbf{d}_G, \theta, y) \equiv F(x_U)$.

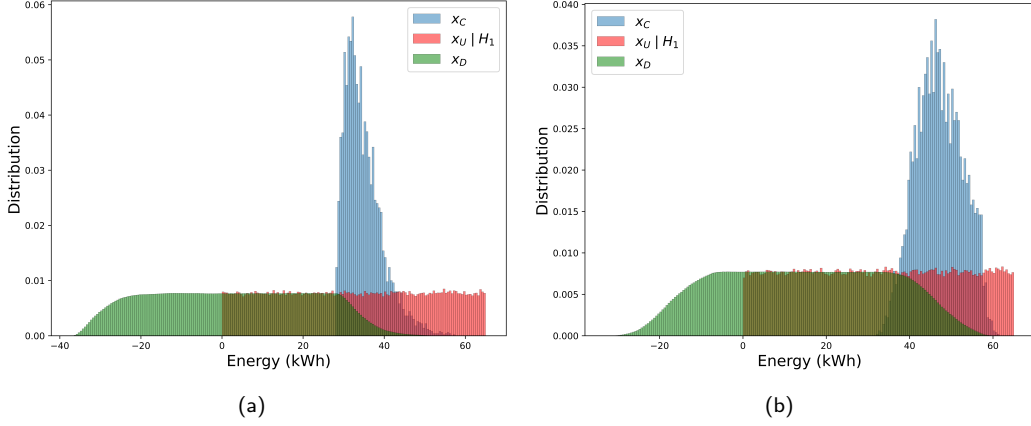


Figure 4: Histogram representations (in green) of the empirical distributions, $\tilde{F}(x_D | \mathbf{d}_G, \theta, y)$ (23), of the certified differential SoC, x_D , in (a) summer ($y = s$), and (b) winter ($y = w$). Also displayed are the contributing distributions in (23), i.e. $\tilde{F}(x_C | \mathbf{d}_G, \theta, y)$ (17) (in blue) and the conditional distribution, $\tilde{F}(x_U | H_1)$ (in red).

3.5 Testing the hypothesis of undeclared charging, H_1

We now compute a Bayesian hypothesis test for H_1 (Section 3.3) via the binary mixture model of x_D (23). As explained near the beginning of Section 3, this involves the sequential¹⁰ processing of (i.e. conditioning on) the measured differential SoC, x_D (15), yielding $\Pr[H_1 | \mathbf{d}_G, \theta, y, x_D]$ (14). It follows from a simple application of Bayes' rule [1]:

$$\Pr[H_1 | \mathbf{d}_G, \theta, y, x_D] = \frac{p_1 \tilde{F}(x_D | \mathbf{d}_G, \theta, y, H_1)}{p_1 \tilde{F}(x_D | \mathbf{d}_G, \theta, y, H_1) + (1 - p_1) \tilde{F}(x_D | \mathbf{d}_G, \theta, y, H_0)}. \quad (27)$$

The components on the right-hand-side of (27) are evaluated at the observed x_D via (24) and (26).

4 Simulation results for the Bayesian test of the undeclared charging hypothesis, H_1

In this section, we present extensive simulations to validate the Bayesian hypothesis testing framework—which we will call the “algorithm”—defined via (27). For this purpose, we deploy the popular mobility simulator, SUMO, to reproduce a road network and its traffic. We use the resulting simulated data to validate the algorithm under controlled conditions. Section 4.1 briefly presents the mobility simulator and the selected case study, while Section 4.2 reports the performance of the algorithm under different operating conditions.

¹⁰The inference is sequential, in that have already processed the EV-specific database from the certified interval, i.e. $(\mathbf{d}_G, \theta, y)$. In this sense, $\tilde{F}(x_D | \mathbf{d}_G, \theta, y)$ (23) is a data-informed prior for X_D , and we wish then to soft-classify (i.e. infer the label of) the observed $X_D = x_D$.

4.1 The SUMO mobility simulator

SUMO (Simulation of Urban MObility) [18] is a microscopic and continuous multi-modal traffic simulation platform that has been designed to handle and analyse large traffic networks. Several key inputs are required, which we instantiate in our current work as described next:

- *Simulation environment*: our simulated road network covers part of *central London*. It is imported using OpenStreetMap [26], an editable map database. We have divided the road network into 11 distinct areas, as depicted in Figure 5.

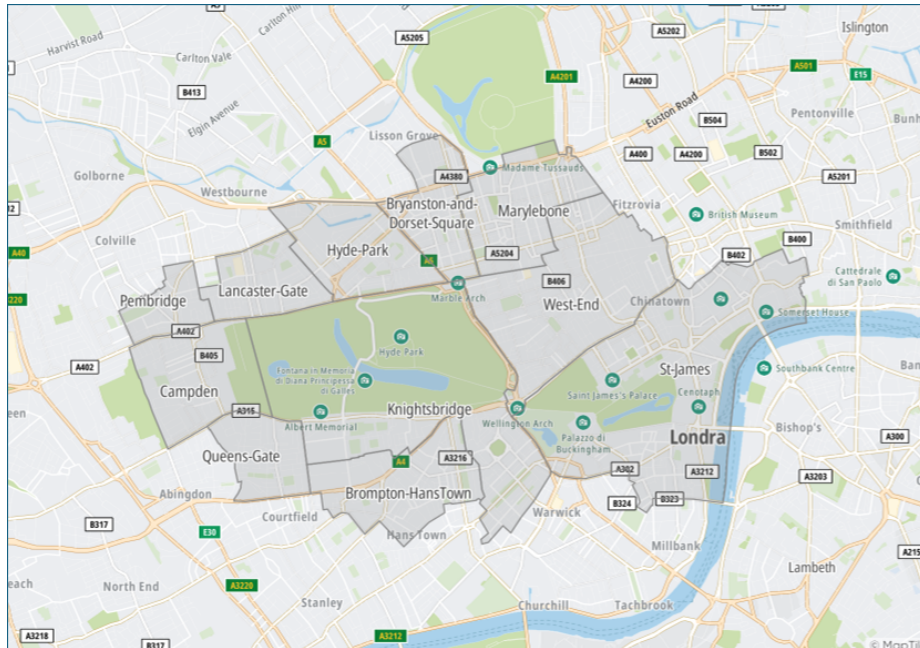


Figure 5: Map of the neighbourhoods of London (UK) which have been used for our case study. The map has been imported through OpenStreetMap [26].

- *EV properties*: recall that the algorithm must have access to the parameters, θ , of the specific EV (Table 1). For simplicity, we adopt θ for the KIA Soul EV 2020 (Table 3), this being the default compact EV model in the *electric* class of SUMO.

Parameter	Symbol	Value
Battery capacity	E_{max}	35 kWh
Kerb mass	m_{veh}	1682 kg
Front surface area	A_{veh}	2.6 m ²
Internal moment of inertia	J_{int}	40 kg.m ²
Radial drag coefficient	c_{rad}	0.1
Roll drag coefficient	c_{roll}	0.01
Air drag coefficient	c_w	0.35
Propulsion efficiency	η_{prop}	0.98
Recuperation efficiency	η_{recup}	0.96

Table 3: Specific EV parameters (for the KIA Soul EV 2020), θ , used in the SUMO-based simulations.

- *Origin-destination (OD) matrix*: the entries in this 11×11 matrix record the numbers of trips between the 11 origin areas—indexing the rows of the matrix—and (the same 11) destination areas—i.e. matrix columns—in central London (Figure 5). The OD matrix is used to simulate traffic flows by specifying the number of EVs that travel between the areas of the road network in a specific time frame. An example of this OD matrix for one hour is provided in Figure 6. In principle, these OD matrices are available to city municipalities via sensing infrastructure and surveys. The OD matrix in Figure 6 was generated using the TomTom O/D Analysis API [36]. This API analyzes historical traffic data using *floating car data* (FCD) from millions of anonymized TomTom navigation devices and apps, providing realistic insights into traffic flows and patterns. The numbers of trips reported in Figure 6 have been proportionally down-scaled to simulate traffic-free conditions.

		DESTINATIONS										
		Queens-...	Brompto...	Camden	Pembridge	St-James	Lancaste...	Knightsbr...	Hyde-Park	West-End	Bryansto...	Marylebo...
ORIGINS	Queens-Gate	262	202	51	23	303	11	182	31	122	16	31
	Brompton-HansT...	164	307	14	10	58	5	99	16	68	20	34
	Camden	52	16	193	54	41	22	34	8	26	11	16
	Pembridge	31	34	266	242	17	41	27	17	12	8	26
	St-James	259	77	16	10	1793	18	82	93	214	27	62
	Lancaster-Gate	10	10	29	14	25	96	16	40	18	7	30
	Knightsbridge	155	81	34	16	165	40	263	204	135	54	88
	Hyde-Park	16	22	22	16	116	133	46	497	75	54	56
	West-End	32	25	5	2	141	13	34	45	206	50	85
	Bryanston-and-...	9	65	2	0	355	15	98	234	178	410	701
	Marylebone	21	40	11	8	99	24	27	627	179	94	462

Figure 6: The OD matrix generated via the *TomTom O/D Analysis API* [36] for the time frame 08:00-09:00 on Monday 24th October 2022.

Recall, from Section 2, that the cumulative energy drawn from the battery during a trip of t s, i.e. $x_C[t]$ (8), is evaluated in discrete time, $t \in \{0, 1, 2, \dots\}$ s, via the physical model (1)-(7). This is consistent with the model deployed by the *electric* class in SUMO. Hence, the SUMO simulations are conducted in discrete time, using a one-second time step (Table 2).

4.2 Performance of the hypothesis test for undeclared charging

In Figure 7, we display $\Pr[H_1 | \mathbf{d}_G, \theta, y, x_D] \equiv \Pr[H_1 | \cdot, x_D]$ (27) (being the probability that at least one undeclared charging event occurred during the certified interval) as a function of x_D (15) (i.e. the measured differential SoC for the interval). The certified interval duration, T_C (Section 3), is set at about two weeks, corresponding to about 40 trips, each about 8 km long (i.e. a total of about 320 km in two weeks).

The dependence of $\Pr[H_1 | \cdot, x_D]$, on the season, $Y = y \in \{s, w\}$, is evident in Figure 7. In both cases, $\Pr[H_1 | \cdot, x_D] \rightarrow 1$, for low values of x_D , i.e. for those differential SoCs which are inconsistent with the GPS record (Table 2), and, therefore, inconsistent with the values of x_C that are probable under (17). Meanwhile, $\Pr[H_1 | \cdot, x_D] \rightarrow 0$ as x_D increases to values with high probability under H_0 (25). Note the more rapid transition in $\Pr[H_1 | \cdot, x_D]$ in summer than in winter. This is caused by the increased uncertainty in x_C (17) in winter (see Figure 3), which, in turn, is induced by the increased uncertainty of W in winter (i.e. in the power drawn by the heating system) compared to W in summer (i.e. drawn by the A/C system). In Figure 7, we have indicated the seasonal cases when $x_D = x_{C, \text{MAP}}$, i.e. the modal values of x_C , respectively (see Figure 3). This verifies the satisfactory performance of the algorithm, which assigns high probabilities to H_0 (i.e. to the hypothesis that no undeclared charging occurred) in this case. An empirical study of the performance of the algorithm follows in Section 4.4.

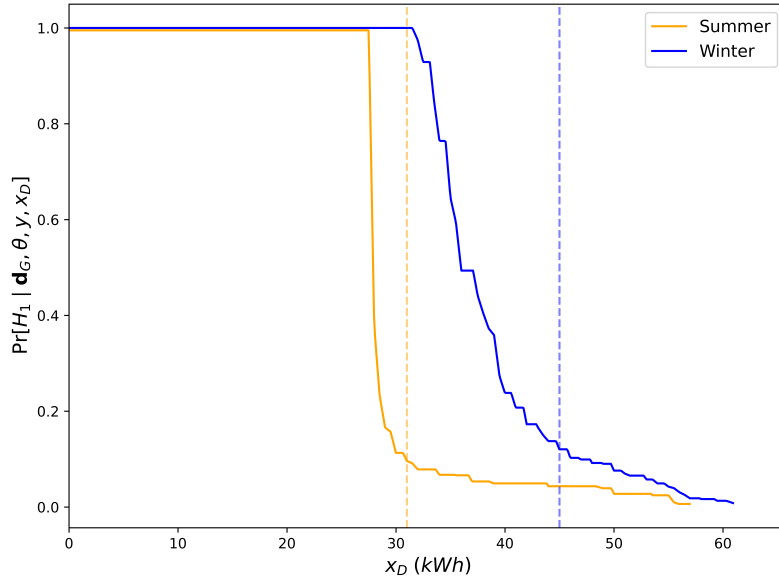


Figure 7: Probability of undeclared charging, $\Pr[H_1 | \cdot, x_D]$, as a function of the certified differential SoC, x_D . The dotted lines indicate $x_D \equiv x_{C, \text{MAP}}$ for the respective seasons (see Figure 3).

4.3 The hypothesis test in representative scenarios

We now describe how $\Pr[H_1 | \cdot, x_D]$ (27)—which has been graphed as a function of the measured differential SoC, x_D , for the two seasonal cases, $y \in \{s, w\}$, in Figure 7—can be deployed in the detection of various non-compliant behaviours (i.e. uncertified charging) by drivers.

4.3.1 Scenario 1: H_1 true, with $x_U = 0.5 E_{max}$ (Figure 8)

Here, we simulate x_D when undeclared charging has, indeed, taken place, the amount of undeclared charge being 50% of the battery capacity, E_{max} (Table 3: see Footnote 9). In this flagrant non-compliance case, the measured differential SoC (15) is probably small. Indeed, there is a strictly positive probability that $x_D < 0$, as seen in summer (Figure 8(a)). Such values of x_D provide trivial tests for the algorithm (see Footnote 8). Meanwhile, the hypothesis test correctly detects the undeclared charging event(s) for all simulated cases of x_D ; i.e. note that $\Pr[H_1 | \cdot, x_D] \rightarrow 1$ across the entire range of simulated x_D in this scenario. In Section 4.4, we will quantify the sensitivity of the test.

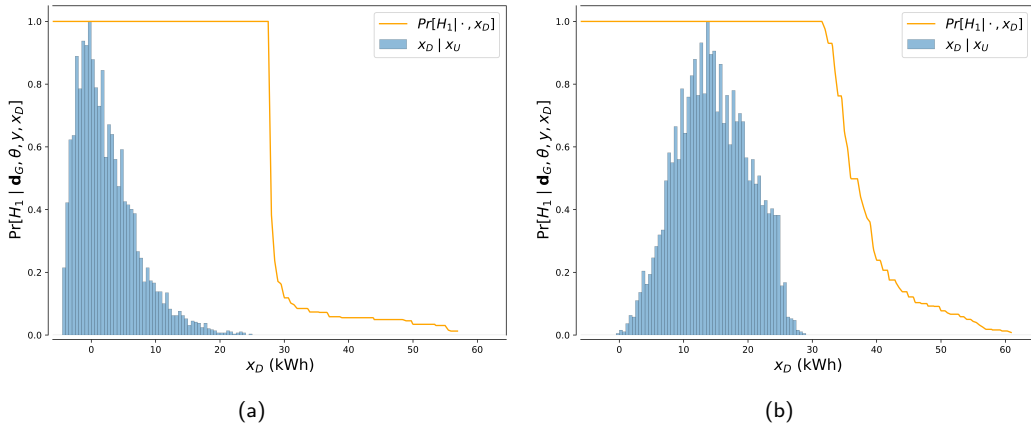


Figure 8: Probability of undeclared charging, $\Pr[H_1 | \cdot, x_D]$, when *significant undeclared charging* has occurred (i.e. H_1 , with $x_U = 0.5 E_{max}$), in (a) summer, and (b) winter. The empirical distribution of $x_D | x_U$ is superimposed in each case.

4.3.2 Scenario 2: H_0 true, i.e. $x_U = 0$ (Figure 9)

We repeat the investigation when the driver has definitely been compliant with the charge certification scheme, in the sense that they have not charged their EV during the certified interval. The same GPS data, \mathbf{d}_G , are adopted as in scenario 1. Hence, the consumed energy distribution, $\tilde{F}(x_C | \mathbf{d}_G, \theta, y)$ (17), is the same as in scenario 1. For the same reason, the Bayesian hypothesis test, $\Pr[H_1 | \mathbf{d}_G, \theta, y, x_D]$ (27) is also invariant. The test performs excellently once again; i.e. $\Pr[H_1 | \cdot, x_D] \rightarrow 0$ for most simulated cases of x_D when $x_U = 0$. This is so because these x_D s are, by definition (15), iid draws from the x_C predictor. Nevertheless, false positives do occur, particularly in winter. The core reason for this is the increased uncertainty around the use of auxiliary services, i.e. W , evident in Figure 2. There is a significant probability of low W (5) in winter (i.e. drivers may choose not to use the heating system during mild periods), and, therefore, low x_D , in which case $\Pr[H_1 | \cdot, x_D] \gg 0$. We will assess the specificity of the test in Section 4.4.

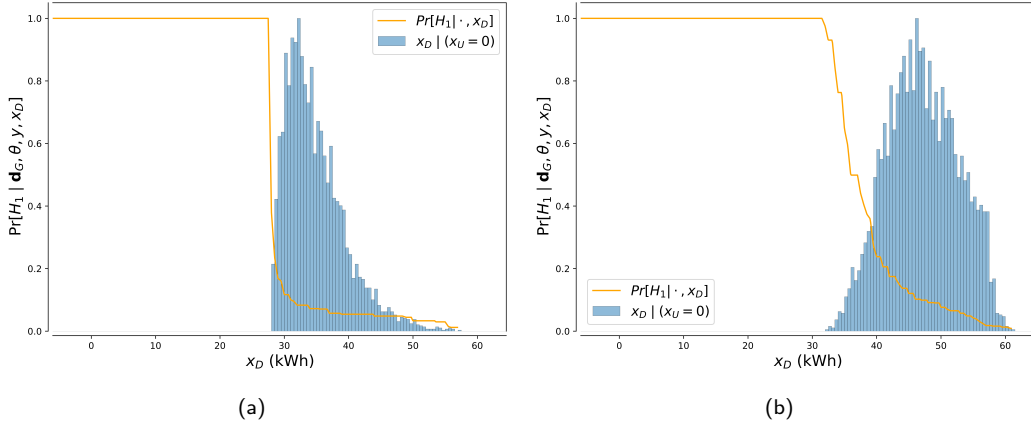


Figure 9: Probability of undeclared charging, $\Pr[H_1|\cdot, x_D]$, when there has been *no undeclared charging* (i.e. $H_0 \equiv (x_U = 0)$), in (a) summer, and (b) winter. The empirical distribution of $x_D | (x_U = 0)$ is superimposed in each case. They are respectively equal to $\tilde{F}(x_C | \mathbf{d}_G, \theta, y)$ (17) in this H_0 case.

4.3.3 Scenario 3: H_1 true, with $x_U = 0.2 E_{max}$ (Figure 10)

Finally, we illustrate in Figure 10 the situation when drivers engage in a small amount of undeclared charging, i.e. $x_U = 0.2 E_{max}$. Once again, the GPS data, \mathbf{d}_G , remain invariant. These—perhaps deliberate—cases of minor non-compliance with the certification scheme are unsurprisingly harder to detect, particularly in winter, when uncertainty around the use of auxiliary devices causes $\Pr[H_1|\cdot, x_D] \ll 1$ in a significant proportion of the simulated cases of x_D .

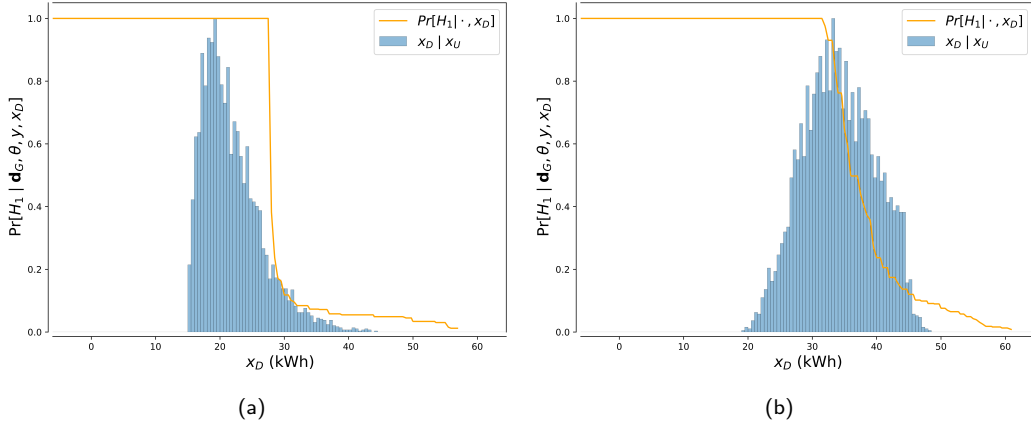


Figure 10: Probability of undeclared charging, $\Pr[H_1|\cdot, x_D]$, when *minor undeclared charging* has occurred (i.e. H_1 , with $x_U = 0.2 E_{max}$), in (a) summer, and (b) winter. The empirical distribution of $x_D | x_U$ is superimposed in each case.

In summary, the behaviour of the Bayesian hypothesis test is evident from these scenarios, all of which involve the same SUMO-simulated EV trips during the certified interval. The empirical distribution of

x_D is invariantly shifted by the amount of $x_U \geq 0$; i.e. inserting the energy conservation equation (15) into (23), then

$$\tilde{F}(x_D | \mathbf{d}_G, \theta, y, x_U) = \tilde{F}(x_C | \mathbf{d}_G, \theta, y) \Big|_{x_C \rightarrow x_D + x_U}.$$

Meanwhile, the Bayesian classifier, $\Pr[H_1 | \mathbf{d}_G, \theta, y, x_D]$ (27) is, of course, not a function of x_U , since the latter has been marginalized out via (24) and (25).

4.4 Statistical Performance of the Test for Undeclared Charging

Having gained an understanding of the behaviour of the testing algorithm for specific amounts of undeclared charging ($x_U > 0$ given H_1 and $x_U = 0$ given H_0 (19)), we want to assess its statistical performance—such as its sensitivity and specificity—under predictable behaviours of the driver. For this purpose, we hierarchically draw iid samples from the slab-and-spike mixture model of x_U (22) in a Monte Carlo (MC) simulation. We first simulate from the noninformative (i.e. unbiased) Bernoulli prior for H_1 (19), with $p_1 \equiv 0.5$ (i.e. we have no prior opinion as to whether the driver has been engaging in undeclared charging during the certified interval). If H_1 is realized, then we draw from (20), with $\bar{x}_U \equiv E_{max}$ (Table 3). If H_0 , then we set $x_U = 0$. We undertake 10,000 such trials for each of $y \in \{s, w\}$ (Section 2.3.2), so that approximately 5,000 are H_1 trials, and 5,000 are H_0 trials, in each season. In all these trials, we hold the traffic (\mathbf{d}_G) and EV (θ) operating conditions constant, and so the seasonally-adjusted empirical distributions, $\tilde{F}(x_C | \mathbf{d}_G, \theta, y)$, of cumulative energy drawn from the battery, x_C , during the (multi-trip) certified interval is invariant across the trials, being those adopted in the scenarios above (Figure 9).

Recall that this is a Bayesian hypothesis test, yielding the *a posteriori* probability, $\Pr[H_1 | \mathbf{d}_G, \theta, y, x_D]$, as its natural output. We assess the performance of the test via the empirical distributions (histograms) of $\Pr[H_1 | \cdot, x_D]$ for the two prior cases of the driver (H_1 and H_0), and for the two seasons (Figure 11).

Clearly, the test performs excellently in discriminating between the two cases, H_1 (undeclared charging took place during the certified interval) and H_0 (there was no undeclared charging). It should be noted that this MC simulation study was performed under conservative—and therefore testing—conditions, in which there is a high probability of behaviour aimed at fooling the algorithm; i.e. $H_1 = 1$ and $x_U \ll E_{max}$ (as studied in scenario 2). For example, $\Pr[x_U < 0.5E_{max} | H_1] \equiv 0.5$ (20), owing to the conservative uniform prior elicitation of $F(x_U | H_1)$ (20) (see the red histograms in Figure 4).

In the prior- H_1 cases (Figure 11), $\Pr[H_1 | \mathbf{d}_G, \theta, y, x_D] = 1$ with high probability. Nevertheless, we note that—with probabilities of about 0.2—the test computes $\Pr[H_1 | \cdot, x_D] \ll 1$. This is a consequence of the case demonstrated in scenario 2, in which a driver typically attempts to fool the test by charging to a low proportion of E_{max} during the certified interval.

In the prior H_0 cases, there is no confounding with H_1 (i.e. $\Pr[H_1 | \mathbf{d}_G, \theta, y, x_D] \ll 1$ always), but there is more statistical uncertainty in these probabilities. This is a function of the intrinsic (and modelled) uncertainty in the passenger-loading of the EV (10) and in the driver's use of the auxiliary devices (11), particularly in winter (Figure 2).

If a hard H_1 -vs- H_0 decision is to be implemented, then this is done by thresholding the *a posteriori* probabilities, $\Pr[H_1 | \mathbf{d}_G, \theta, y, x_D]$ (27), in an appropriate manner. We censor equivocal inferences by designing a ternary decision, involving an erasure (i.e. censored) state, E , in which case no decision about the behaviour of the driver is made:

$$\Pr[H_1 | \mathbf{d}_G, \theta, y, x_D] \in \begin{cases} [0, 0.4] & \Rightarrow H_0, \\ (0.6, 1.0] & \Rightarrow H_1, \\ \text{otherwise} & \Rightarrow E. \end{cases} \quad (28)$$

We implement this for each of the 10,000 trials (for each season) of the MC simulation (Figure 11), yielding the seasonally dependent confusion matrices in Figure 12. Conditional on erasure of the E states, these statistics yield test sensitivities of 89% in summer and 85.8% in winter. The specificities of the test are 100% and 98.7%, respectively.

In order to validate the proposition, above, regarding the conservative (i.e. stressful) operating conditions which have been implemented in our MC simulations (Figures 11 and 12)—where 50% of cases of undetected charging are ‘small’ (i.e. $x_U \leq 0.5E_{max}$)—we adjust the range of $x_U | H_1$ in (20) to $(0.2E_{max}, E_{max}]$, reducing the probability that undeclared charging is small to 38%. As predicted, the performance of our Bayesian hypothesis test of undeclared charging is then even better (Figure 13), with the sensitivities rising to 99.2% and 97%, respectively, while the specificities rise to 100% and 99.4%, respectively.

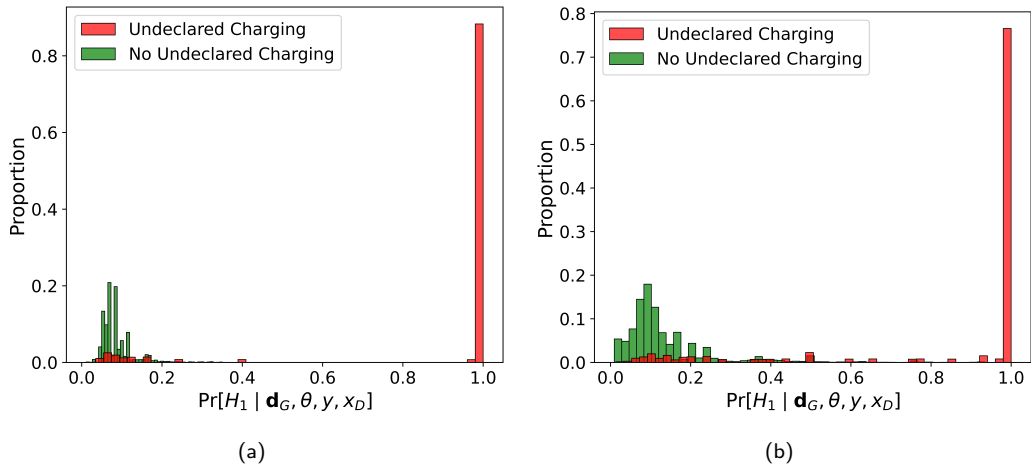


Figure 11: Histograms of 10,000 trials, in (a) summer, and (b) winter, of the Bayesian hypothesis test for undeclared charging, illustrating $\Pr[H_1 | \mathbf{d}_G, \theta, y, x_D]$ in each case. These are segmented into the cases in which there has, indeed, been undeclared charging during the certified interval (i.e. H_1 , in red), and those in which there was no undeclared charging (H_0 , in green).

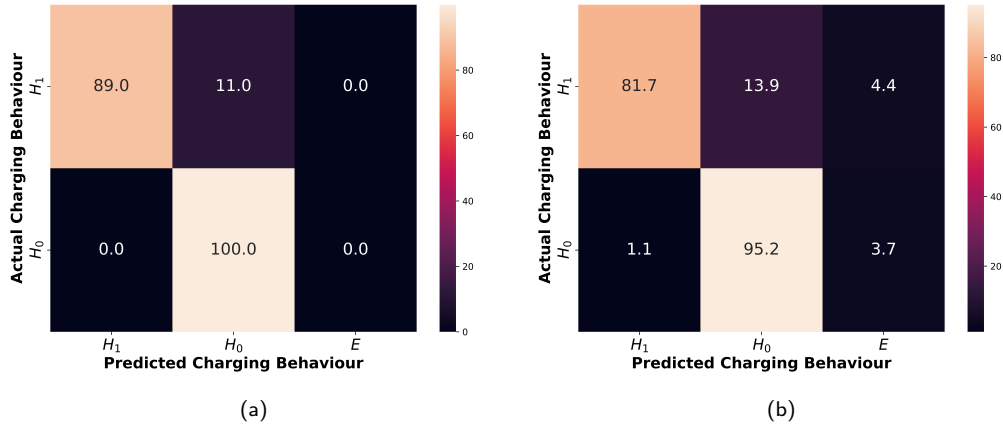


Figure 12: Confusion matrices of the Bayesian hypothesis test in (a) summer, and (b) winter, when $x_U | H_1 \in (0, E_{max})$, as in Figure 11. The matrices record the ternary decision (28) percentages for both types of driver behaviour.

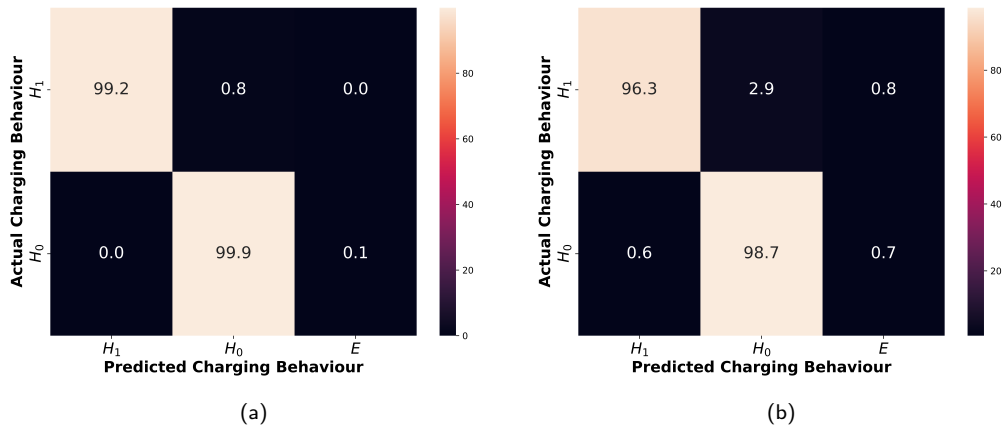


Figure 13: Confusion matrices of the Bayesian hypothesis test in (a) summer, and (b) winter, when $x_U | H_1 \in (0.2E_{max}, E_{max})$. The matrices again record the ternary decision (28) percentages for both types of driver behaviour.

5 Discussion and concluding remarks

There are several benefits attached to the Bayesian formulation (27) of the test for undeclared charging:

- (i) The algorithm calculates the EV's *a posteriori* probability (27), and provides it to the operator of the green-energy certification scheme, as soon as it is connected to the next charging station belonging to the scheme. As we have seen (28), this can be used to make a decision as to whether the EV was subject to undeclared—and therefore possibly not green-energy—charging since the last certified charging event. This decision can be used to apply or withhold either an incentive/bonus

or a penalty/levy applied to the driver by the operator of the scheme. However, a fairer approach is to use this probability to *weight* the bonus or levy. For instance, in an incentivization scheme, a simple approach would be to apply the bonus, $(1 - \Pr[H_1 | \cdot, x_D])G$, where G is the maximal bonus for compliance with the scheme—when the EV is charged at a certified charging station.

- (ii) The sequential nature of Bayesian inference allows probabilities to be propagated from one certified interval to the next. The *a posteriori* probability, $\Pr[H_1 | \cdot, x_D]$ (27), can be assigned as the *priori* probability, $p_1 \equiv \Pr[H_1]$ (19), for the next charging interval. Again, a fairer scheme would seek to model non-stationarity in the driver’s behaviour over time. One approach involves the estimation of a forgetting factor, $0 \leq \lambda \leq 1$, based on an assessment of the pseudo-stationary window-length of the driver’s behaviour (high λ corresponding to slow change in behaviour) [40], so that

$$p_{1,i+1} \equiv \lambda \Pr_i[H_1 | \cdot, x_D],$$

where i indexes the sequence of certified charging intervals. There is more work to be done in modelling nonstationary dynamics in the driver’s behaviour with respect to the certification scheme. Indeed, the same sequential inference procedure could also be used to sharpen the undeclared charging prior, $F(x_U | H_1)$ (20), by updating it to the *a posteriori* distribution, $F(x_U | \mathbf{d}_G, \theta, y, x_D, H_1)$, based on the evidence from the last certified interval. This would then be propagated forward (perhaps with forgetting) as the $x_U | H_1$ prior (20) for the next interval.

- (iii) The parametric Bayesian framework of this paper requires all stochastic modelling assumptions, and the knowledge base, $\{\mathbf{d}_G, \theta, y, x_D\}$, to be explicitly declared. This facilitates the potential inclusion of other factors into the methodology, such as the effect of per-unit green-energy price volatility on x_U , which can be processed into the prior, $F(x_U | H_1)$ (20). In this paper, we have adopted noninformative or conservative prior parameters in several instances, such as in $F(m_{peop})$ (10) and $F(W | y)$ (11), as well as in $F(x_U | H_1)$ (20). These could all be further data-informed by recourse to publicly available—or driver-supplied—knowledge.

On this last point, we have noted (in scenario 2 in Section 4.3.3) that low- x_U undeclared charging can lead to false negatives in a small number of cases (see Figure 11(b), and the top row of the confusion matrix in Figure 12(b)). We see different—potentially deleterious—effects of uncertainty in the heavy right-tails of the $\Pr[H_1 | \cdot, x_D]$ distributions in the H_0 cases (Figure 11). While these tails do not incur a significant rate of false-positives, the problem is again caused by the significant uncertainty engendered in the consumed energy predictor, $\tilde{F}(x_C | \mathbf{d}_G, \theta, y)$ (17), particularly because of the uncertainties in auxiliary power, W (11). In common with *loyalty schemes*, widely adopted in retail, our framework can be adapted to provide a further bonus to drivers who cooperate in sharing data that improve the statistical performance of the predictor. As ever, the cost to the driver—in terms of loss of privacy—needs to be assessed in any fair implementation of the scheme that relies on private-data-driven elicitation of the priors.

Finally, in order to support the incentivization scheme based on our detection algorithm, it would be necessary to implement it on a *distributed ledger technology (DLT)* platform, such as blockchain. This would enable secure, transparent, and tamper-proof recording of charging events by drivers and their energy consumption data. Smart contracts could be developed, which would apply rewards automatically, based on processing verified charging data, thereby enhancing trust and reducing administrative effort.

5.1 Concluding remarks

The paper has developed a novel methodology for Bayesian detection of undeclared charging events for use in a green-energy certification scheme. Simulated GPS data, EV parameters and the measured

differential SoC have been processed into a probability of undeclared charging during intervals between certified charging events. Extensive simulations have demonstrated the excellent statistical performance of the approach under realistic operating conditions. We have outlined how the Bayesian formulation of the test can serve the needs of an incentivization scheme for green-energy consumption, and how it can readily exploit other knowledge sources.

References

- [1] A. Papoulis. *Probability, random variables, and stochastic processes*. McGraw-Hill, 1991.
- [2] Y. Al-Wreikat, C. Serrano, and J. R. Sodré. Effects of ambient temperature and trip characteristics on the energy consumption of an electric vehicle. *Energy*, 238:122028, 2022.
- [3] P. Barman, L. Dutta, S. Bordoloi, A. Kalita, P. Buragohain, S. Bharali, and B. Azzopardi. Renewable energy integration with electric vehicle technology: A review of the existing smart charging approaches. *Renewable and Sustainable Energy Reviews*, 183:113518, 2023.
- [4] M. Behrisch, L. Bieker, J. Erdmann, and D. Krajzewicz. SUMO-simulation of urban mobility: an overview. In *Proceedings of SIMUL 2011, The Third International Conference on Advances in System Simulation*. ThinkMind, 2011.
- [5] J. M. Bernardo and A. Smith. *Bayesian Theory*. Wiley series in probability and statistics. Wiley, 2000.
- [6] J. Brady and M. O'Mahony. Development of a driving cycle to evaluate the energy economy of electric vehicles in urban areas. *Applied energy*, 177:165–178, 2016.
- [7] A. Braun and W. Rid. The influence of driving patterns on energy consumption in electric car driving and the role of regenerative braking. *Transportation Research Procedia*, 22:174–182, 2017.
- [8] S. Chang, Y. Niu, and T. Jia. Coordinate scheduling of electric vehicles in charging stations supported by microgrids. *Electric Power Systems Research*, 199:107418, 2021.
- [9] A. Donkers, D. Yang, and M. Viktorović. Influence of driving style, infrastructure, weather and traffic on electric vehicle performance. *Transportation Research Part D: Transport and Environment*, 88:102569, 2020.
- [10] Eurostat. Passenger mobility statistics. https://ec.europa.eu/eurostat/statistics-explained/index.php?title=Passenger_mobility_statistics#Passenger_car_occupancy, 2021.
- [11] I. Evtimov, R. Ivanov, and M. Sapundjiev. Energy consumption of auxiliary systems of electric cars. In *MATEC web of conferences*, volume 133, page 06002. EDP Sciences, 2017.
- [12] Y. Gu, F. Häusler, W. Griggs, E. Crisostomi, and R. Shorten. Smart procurement of naturally generated energy (SPONGE) for PHEVs. *International Journal of Control*, 89(7):1467–1480, 2016.
- [13] IEA and AIE. *Global ev outlook 2023: Catching up with climate ambitions*. OECD Publishing, 2023.
- [14] J. Jaguemont, L. Boulon, and Y. Dubé. A comprehensive review of Lithium-ion batteries used in hybrid and electric vehicles at cold temperatures. *Applied Energy*, 164:99–114, 2016.

- [15] M. Jakob. Why carbon leakage matters and what can be done against it. *One Earth*, 4(5):609–614, 2021.
- [16] M. Kajanova and P. Bracinik. Social welfare-based charging of electric vehicles in the microgrids fed by renewables. *International Journal of Electrical Power and Energy Systems*, 138:107974, 2022.
- [17] K. R. Kambly and T. H. Bradley. Estimating the hvac energy consumption of plug-in electric vehicles. *Journal of Power Sources*, 259:117–124, 2014.
- [18] T. Kurczveil, P. Á. López, and E. Schnieder. Implementation of an energy model and a charging infrastructure in sumo. In *Simulation of Urban Mobility: First International Conference, SUMO 2013, Berlin, Germany, May 15-17, 2013. Revised Selected Papers 1*, pages 33–43. Springer, 2014.
- [19] K. Liu, J. Wang, T. Yamamoto, and T. Morikawa. Modelling the multilevel structure and mixed effects of the factors influencing the energy consumption of electric vehicles. *Applied energy*, 183:1351–1360, 2016.
- [20] K. Liu, J. Wang, T. Yamamoto, and T. Morikawa. Exploring the interactive effects of ambient temperature and vehicle auxiliary loads on electric vehicle energy consumption. *Applied Energy*, 227:324–331, 2018.
- [21] K. Liu, T. Yamamoto, and T. Morikawa. Impact of road gradient on energy consumption of electric vehicles. *Transportation Research Part D: Transport and Environment*, 54:74–81, 2017.
- [22] A. K. Madhusudhanan and X. Na. Effect of a traffic speed based cruise control on an electric vehicle's performance and an energy consumption model of an electric vehicle. *IEEE/CAA Journal of Automatica Sinica*, 7(2):386–394, 2020.
- [23] McKinsey. Scaling EV infrastructure to meet net-zero targets. Technical report, McKinsey & Company, October 2021.
- [24] A. Millard-Ball and L. Schipper. Are we reaching peak travel? trends in passenger transport in eight industrialized countries. *Transport reviews*, 31(3):357–378, 2011.
- [25] M. R. Mozafar, M. H. Moradi, and M. H. Amini. A simultaneous approach for optimal allocation of renewable energy sources and electric vehicle charging stations in smart grids based on improved GA-PSO algorithm. *Sustainable cities and society*, 32:627–637, 2017.
- [26] OpenStreetMap contributors. Planet dump retrieved from <https://planet.osm.org> . <https://www.openstreetmap.org>, 2017.
- [27] S. W. Park, K. S. Cho, G. Hoefter, and S. Y. Son. Electric vehicle charging management using location-based incentives for reducing renewable energy curtailment considering the distribution system. *Applied Energy*, 305:117680, 2022.
- [28] N. Piao, X. Gao, H. Yang, Z. Guo, G. Hu, H. M. Cheng, and F. Li. Challenges and development of Lithium-ion batteries for low temperature environments. *Etransportation*, 11:100145, 2022.
- [29] A. H. Salari, H. Mirzaeinejad, and M. F. Mahani. A new control algorithm of regenerative braking management for energy efficiency and safety enhancement of electric vehicles. *Energy Conversion and Management*, 276:116564, 2023.
- [30] J. Soares, M. A. F. Ghazvini, N. Borges, and Z. Vale. Dynamic electricity pricing for electric vehicles using stochastic programming. *Energy*, 122:111–127, 2017.

- [31] All Star. Revealing the real-life cost of petrol, diesel and electric. Technical report, Allstar Business Solutions, Winter 2024.
- [32] D. J. Sun, Y. Zheng, and R. Duan. Energy consumption simulation and economic benefit analysis for urban electric commercial-vehicles. *Transportation Research Part D: Transport and Environment*, 101:103083, 2021.
- [33] T. Q. Tang, H. J. Huang, and H. Y. Shang. Influences of the driver's bounded rationality on micro driving behavior, fuel consumption and emissions. *Transportation Research Part D: Transport and Environment*, 41:423–432, 2015.
- [34] M. Tanner. *Tools for statistical inference*. Springer, 1996.
- [35] S. Tirunagari, M. Gu, and L. Meegahapola. Reaping the benefits of smart electric vehicle charging and vehicle-to-grid technologies: Regulatory, policy and technical aspects. *IEEE Access*, 10:114657–114672, 2022.
- [36] TomTom. TomTom OD matrix analysis. <https://www.tomtom.com/products/origin-destination-matrix-analysis/>, 2022.
- [37] K. Unni and S. Thale. Influence of auxiliary loads on the energy consumption of electric vehicle—a case study. In *2021 IEEE Transportation Electrification Conference (ITEC-India)*, pages 1–6. IEEE, 2021.
- [38] J. Urry. *Offshoring*. Wiley, 2014.
- [39] R. Valentina, A. Viehl, O. Bringmann, and W. Rosenstiel. HVAC system modeling for range prediction of electric vehicles. In *2014 IEEE Intelligent Vehicles Symposium Proceedings*, pages 1145–1150. IEEE, 2014.
- [40] V. Šmídl and A. Quinn. Bayesian estimation of non-stationary AR model parameters via an unknown forgetting factor. In *Proc. IEEE Workshop on Dig. Sig. Process.*, pages 221–225. IEEE, 2004.
- [41] S. C. Walpole, D. Prieto-Merino, P. Edwards, J. Cleland, G. Stevens, and I. Roberts. The weight of nations: an estimation of adult human biomass. *BMC public health*, 12:1–6, 2012.
- [42] Z. Wang, G. Feng, D. Zhen, F. Gu, and A. Ball. A review on online state of charge and state of health estimation for Lithium-ion batteries in electric vehicles. *Energy Reports*, 7:5141–5161, 2021.
- [43] C. Will, F. Zimmermann, A. Ensslen, C. Fraunholz, P. Jochem, and D. Keles. Can electric vehicle charging be carbon neutral? Uniting smart charging and renewables. *Applied Energy*, 371:123549, 2024.
- [44] T. Wu, S. Liu, Z. Wang, and Y. Huang. SOC and SOH joint estimation of Lithium-ion battery based on improved particle filter algorithm. *Journal of Electrical Engineering and Technology*, 17(1):307–317, 2022.